Risk Reduction Testing of Superconducting Coils for the High Efficiency Megawatt Motor

Dr. Justin J. Scheidler* and Thomas F. Tallerico†
NASA Glenn Research Center, Cleveland, Ohio, 44135

William Torres‡
Wolf Creek Federal Services, Cleveland, Ohio, 44135

Wesley Miller§
HX5, LLC, Cleveland, Ohio, 44135

Second generation high temperature superconducting coils provide a very attractive level of performance for use in the field winding of electric machines for aircraft. In order to produce a reliable machine, much care must be taken to prevent damaging these relatively fragile materials due to excessive stress. Thermal stresses due to temperature cycling and mechanical stresses due to centrifugal forces are the most critical for the High Efficiency Megawatt Motor. This paper summarizes two test campaigns that were undertaken to reduce the risks posed by these loads. In one campaign, several superconducting coils were fabricated, thermally cycled up to 50 times, and electrically tested in liquid nitrogen to assess the change in superconductivity metrics throughout thermal cycling. In the other campaign, a full-scale superconducting coil was fabricated, a test article was designed to produce a representative stress environment in the coil, the test article and coil were rotated at room temperature up to a speed of 11,800 rpm, and the superconductivity metrics were measured in liquid nitrogen before and after each rotation. The experimental results demonstrate that the superconducting coils manufactured in-house can survive both thermal cycling and high speed rotation with no appreciable degradation in superconducting performance.

I. Introduction

The exceptional specific power and efficiency of the High Efficiency Megawatt Motor (HEMM) is primarily achieved by utilizing a slotless stator and a self-cooled, superconducting rotor composed of 2nd generation high temperature superconductors (2G HTS) [1–7]. A superconducting field winding conducting DC current has a negligible amount of internal energy loss¶ and can produce magnetic field strengths that greatly exceed those produced by conventional conductors or permanent magnets. However, the use of superconductors introduces a number of challenges. Superconductors must be kept at cryogenic temperatures and the superconducting system must be carefully designed to avoid a loss of superconductivity throughout all thermoelectromagnetic operating conditions. Additionally, the 2G HTS superconductors are fragile compared to copper and aluminum; they are subject to maximum axial strain and minimum bend radius constraints, and care must be taken to avoid appreciable shear stresses and transverse tensile stresses as these will delaminate layers of the composite conductor. HEMM's rotor contains twelve 2G HTS, no-insulation, racetrack coils that rotate at 6,800 rpm (107 m/s tip speed) and each contain about 280 m (about 0.6 kg) of superconductor. This combination of relatively high speed and mass lead to a considerable centrifugal load on the superconductor. Throughout most of HEMM's concept of operations, the centrifugal load, electromagnetic (Lorentz) forces, and thermal forces act simultaneously. In this combined stress environment, the risk of mechanical damage cannot be mitigated by analysis alone. 2G HTS are also significantly more expensive than copper and aluminum conductors. Consequently, to overcome these risks, it is important to conduct sub-component testing prior to full-scale implementation of a design.

*Research Aerospace Engineer, Rotating and Drive Systems Branch, non-member.
†Research Aerospace Engineer, Rotating and Drive Systems Branch, non-member.
‡Electrician, non-member.
§Electrical Engineer, Avionics Branch, non-member.
¶Not including the conventional conductors that supply the superconductor with current from room temperature, such a superconducting field winding only exhibits loss due to the resistive splice joints between superconductor segments and AC losses caused by the alternating magnetic flux that results from non-synchronous harmonic content in the stator current.

This paper summarizes two test campaigns that were completed to reduce the two risks that were deemed to be most critical to HEMM's rotor: mechanical damage to the superconducting coils due to (a) thermal cycling and (b) centrifugal forces.

Findings in the literature [8–10] have demonstrated that the superconductivity properties of high temperature superconducting *coils* can degrade as the coil is thermally cycled multiple times from room temperature (293 K) to operating temperature (≤77 K) and back. The degradation is caused by thermal stresses that increase as the coil is cooled due to the difference in thermal contraction between the superconductor and the epoxy that encapsulates it. The degradation would significantly impact the performance of HEMM, because the effect is more pronounced in coils composed of many turns with relatively tight bend radii [8, 11]. Winding coils "dry" (i.e., with no epoxy) [8] or using epoxy that is loaded with small particles of a material having very low thermal expansion [12] has been shown to result in no discernible degradation; however, lack of degradation has only been demonstrated for up to 8 thermal cycles. Also, winding coils completely dry may be problematic when implemented in the rotor of a high power machine due to potential damage caused by relative motion (e.g., delamination or surface wear resulting from electromagnetic- and rotordynamic-induced mechanical vibrations). Consequently, several coils were fabricated and a suite of tests were conducted to reduce this risk. As the test campaign was carried out, the tested coils increased in complexity from a basic sub-scale, single layer (single pancake) coil to a realistic, full-scale coil with 2 layers (double pancake). In Section II, this paper summarizes the test campaign.

Due to the fragile nature of superconductors, HEMM's rotor must be designed so that the superconducting coil can tolerate the forces that will occur during operation. These operating loads include centrifugal, thermal, and electromagnetic forces. Prior analysis by the HEMM team has shown that, at least for this machine, the centrifugal forces are responsible for the majority of the stress in the superconducting coils [4]. The thermal forces resulting from thermal expansion mismatches impose a small to moderate impact on stresses in the HEMM coils, whereas electromagnetic forces cause a small impact. Typically, stresses and strains can be reliably predicted using the finite element method and then compared to known stress and strain limits. For HEMM's superconducting coils, two challenges add significant uncertainty to that approach.

The first challenge is that each of HEMM's superconducting coils are composed of four individual pancake coils that each contain very thin tapes (about 65 micron thick) wound in a loop 150 times[‖] [1]. A proper analysis of this structure would require that each of the 600 turns in the quadruple pancake coil be explicitly modeled with mechanical contact between adjacent turns. Such a model would be very computationally expensive, and it may be impossible in practice for the contact analysis to numerically converge on a solution. Consequently, HEMM's coils have been simulated by simplifying the coils' geometry [4].

The second challenge of conducting a stress analysis is that very little material strength data is available on these 2G HTS, which are anisotropic composite materials [13]. Manufacturers only specify three mechanical properties: an allowable tensile stress and strain along the conductor's length; and a minimum bend radius. No information is provided regarding the influence of or maximum value of shear stresses or the tensile/compressive strengths in other directions.

The aforementioned challenges introduce a considerable amount of risk to the design of HEMM. This risk cannot be adequately addressed through refined analysis. Accordingly, a set of experiments was deemed necessary to reduce this risk to an acceptable level. The objective of this test campaign was to demonstrate that HEMM's superconducting coils can survive the stresses that will be imparted by the centrifugal forces acting on the coil during full speed operation of the machine. This paper summarizes this suite of tests in Section III, including the design of the test article, the test matrix and testing procedure, and the results.

II. Thermal cycling of stationary superconducting coils

The objective of this test campaign was to fabricate coils composed of 2G HTS with varying complexity and to demonstrate that the coils could survive repeated thermal cycling with an acceptably small or negligible amount of degradation in their superconducting response. A total of nine no-insulation (NI) coils were fabricated and tested. This section summarizes the key results for the two most complex coils - a sub-scale, quadruple pancake coil with 25 turns per layer and a full-scale, double pancake coil with 221 turns per layer[**], as shown in Fig. 1. Both of these coils have current terminals and layer-to-layer superconducting jumpers that match the HEMM design. Additional results for the lower fidelity coils in the test matrix as well as tabulated values of the performance metrics for every coil at each measurement point are presented in [14].

[‖] Earlier designs contained about 220 turns per pancake coil [4].

[**] This number of turns matched the HEMM design at the time. This number was changed in the redesign described in [4].

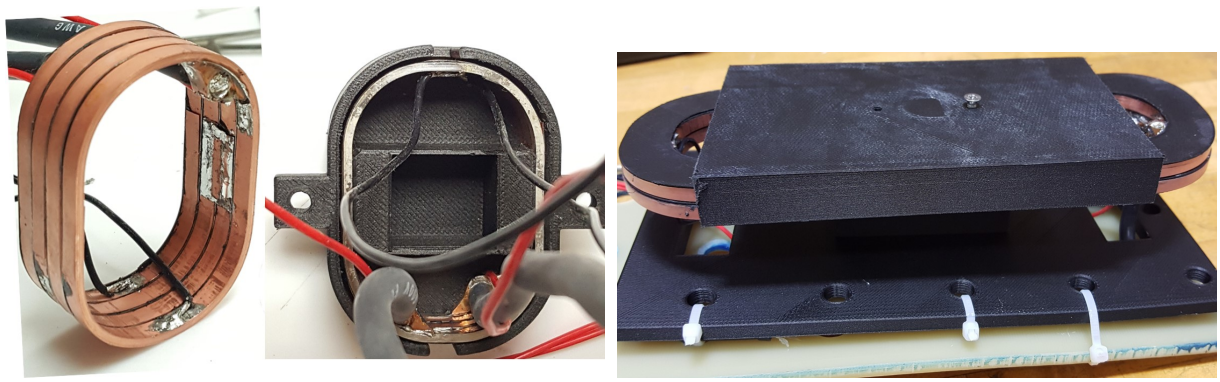

(a) (b)

Fig. 1 Images of two 2G HTS coils used for thermal cycling tests, (a) sub-scale, quadruple pancake coil with 25 turns per layer and (b) a full-scale, double pancake coil with 221 turns per layer.

The experimental method used was to measure the baseline superconducting performance of each coil (i.e., the response after the initial cool down) in liquid nitrogen (LN2) under self field, thermally cycle the coil a given number of times between LN2 and near room temperature, and then re-measure the superconducting performance. The standard superconducting performance metrics - critical current and n-value - were quantified from each electrical characterization measurement to infer whether damage had occurred.

A. Testing procedure

A summary of the procedure is presented here. The detailed procedure is given in the Appendix.

The test was initialized by allowing the electronics to warm up for at least 15 minutes and filling a dewar with LN2. The superconducting coil was then slowly lowered into the LN2 bath, after which electrical connections were made. Next, the voltage versus current response of the coil was measured. For much of the test, this response was measured while the DC current was stepped up and while it was stepped back down. As shown in the following section, the performance metrics for increasing current and decreasing current are nearly the same. Hence, the test concluded by only taking a measurement while the current was increased. Between measurement points, the DC current was ramped up slowly (about 0.1 A/s) to minimize heating in the coil due to AC losses and turn-to-turn current flow. At each current step, a measurement was taken after the voltage reached a steady state.

After the superconducting response was measured, the coil was thermally cycled by warming it up in air then slowly lowering the coil into the LN2 bath and waiting about 5 minutes. The coil's temperature was not measured to ascertain the end of the warm up; however, an air quench and forced convection of room temperature air was used for a consistent and sufficiently long duration to minimize the impact of this limitation. The duration extended about 1 to 2 minutes after the condensation on the coil had evaporated. The superconducting response was measured every 2 to 8 thermal cycles.

B. Summary of performance metrics

Degradation due to thermal cycling is detected by tracking the value of the two most common superconductivity performance metrics – the critical current I_c and the "n-value" n. For a superconductor, a higher value of both the critical current and n-value indicate a higher performing / better quality conductor or coil. These metrics are calculated by fitting the following function to the measured data.

$$\frac{V}{V_c} = \left(\frac{I}{I_c}\right)^n \tag{1}$$

The quantity V_c is the voltage at which the critical current occurs. It is based on an electric field criterion (1 μV/cm) and the total length of superconductor between the two voltage taps. Due to the presence of resistive solder joints connecting the layers of multi-layer coils, the measured voltage includes the superconductor's response (described by the equation above) and a linear Ohmic response. Before fitting the above expression to the data, this linear trend – calculated via a standard least squares regression of only the data in the linear region – is subtracted from the entire measurement, as

demonstrated in Fig. 2. The above expression is only fit to the corrected voltage versus current data that has a high degree of linearity when plotted with a logarithmic voltage scale.

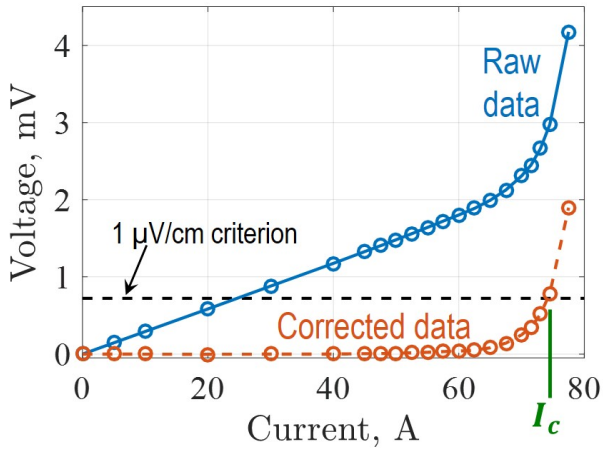

Fig. 2 Example correction of the measured data (blue) to remove the linear Ohmic response of the resistive solder joints and result in the response of the superconductor (red).

For each electrical test, the current was stepped up to slightly above I_c and then stepped down to zero current. Voltage measurements were typically recorded at each step up and each step down. I_c and n were calculated separately for both the increasing current and decreasing current data. This helps to evaluate the experimental uncertainty, and therefore the presence or extent of degradation in the superconducting performance.

For some tests, a prediction of the coil's critical current was determined and compared to the experimental result to further assess whether damage occurred during fabrication or thermal cycling. The prediction was determined by combining data from the superconductor's manufacturer and a finite element simulation, as detailed in [14].

A 6 1/2 digit multimeter was used to measure the coil's voltage with a precision of 0.1 μV using an average of 100 readings. The voltage taps were located at least 10 cm away from each current lead to ensure that the measured current-transfer voltage at the critical current is less than 0.01% of the expected voltage at the critical current, per guidance from [15]. For this test, the applied DC current was measured using the display on the amplifier's front panel, which has a precision of 0.01 A to 0.1 A. For the tests in Section III, the applied DC current was measured using the amplifier's analog current monitor after calibrating its output using a precision, high power resistor and the 6 1/2 digit multimeter.

C. Results and discussion

The performance metrics from testing the sub-scale, four layer coil are shown in Fig. 3. This coil was subjected to a total of 50 thermal cycles. Following the 18th thermal cycle, the test was accelerated by only taking an electrical measurement every 4 to 8 cycles (instead of every 2) and only when the current was increased in steps (instead of for increasing and decreasing current steps). The final 32 thermal cycles were conducted about 1 month after the initial 18. As noted in the figure, the solder joint for a current terminal failed during the measurement after thermal cycle 13, as indicated by an open circuit. Both terminals were re-soldered after this failure, because the joint for the second terminal failed while re-soldering the first. The coil was then reinstalled in the testing fixture and thermal cycling was continued. The performance metrics after fixing the current terminals fall within the same range as the performance metrics in cycles 1 through 9. Hence, it appears that the degraded performance at thermal cycle 11 was likely caused by a partially detached current terminal that fully detached during the measurement at thermal cycle 13. If the data point at thermal cycle 11 is ignored, the remaining data have no clear trend and have a small variation; a linear fit to this data has a negative slope but a very small magnitude and relatively poor correlation coefficient. The critical current values also fall within the predicted range of 60.5 A to 67.5 A [14]. Collectively, these results indicate that no degradation in the superconductor itself occurred during the 50 thermal cycles. However, this test did identify some needed improvements to the quality of the solder joints.

The performance metrics from testing the full-scale, two layer coil are shown in Fig. 4. This coil was subjected to a total of 13 thermal cycles. No issues occurred with the voltage taps or current terminals. Both performance metrics

change little over 13 thermal cycles. A decreasing linear trend in the critical current is observed after the 5th cycle. However, the reduction is only 0.5 A, or 1.5% of the average value, and the final value is still above the first. All values fall within the predicted range of the critical current (32 to 38 A) [14]. Further, over that span, the n-value is nearly constant considering the experimental uncertainty in that metric. Correspondingly, it was concluded that no measurable degradation occurred during this testing.

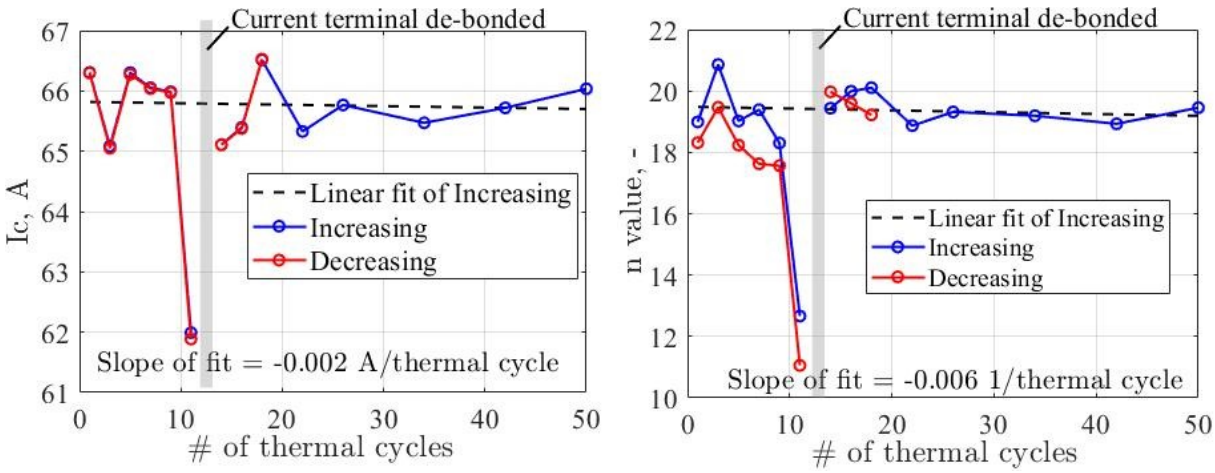

(a) (b)

Fig. 3 Performance metrics of the sub-scale, quadruple pancake coil throughout the thermal cycles.

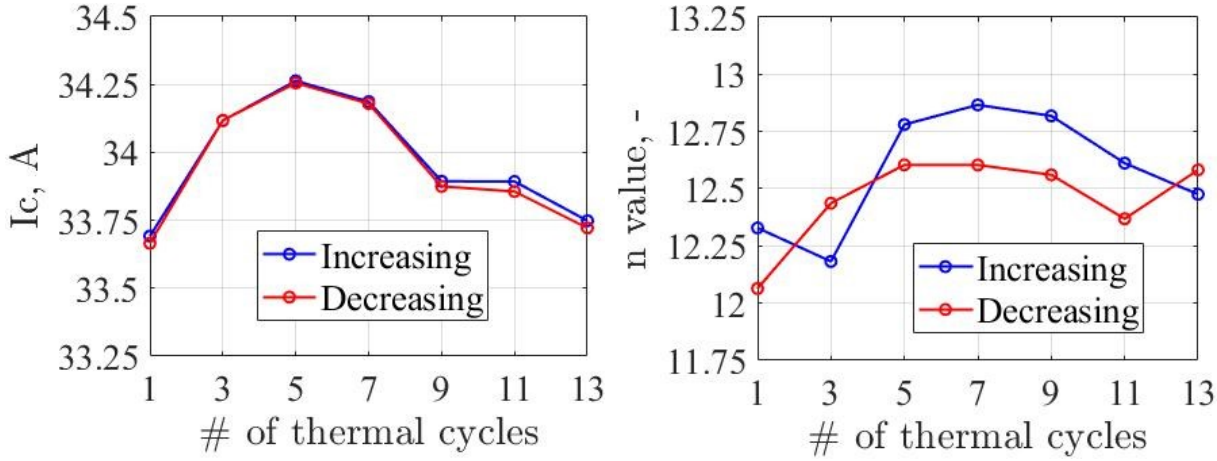

(a) (b)

Fig. 4 Performance metrics of the full-scale, double pancake coil throughout the thermal cycles.

III. Superconducting coils under high speed rotation

The objective of this test campaign was to demonstrate that a full-scale 2G HTS coil fabricated in house could survive a stress environment produced by centrifugal loading that is representative of the HEMM superconducting coil's operating stress environment. The overall approach was to mechanically design a test article that produced a representative stress environment in the coil, fabricate an accurate full-scale, 2 layer (double pancake) coil, spin the test article at select rotational speeds, and measure the superconducting characteristics of the coil before and after each rotation to detect degradation. This section summarizes this test campaign and discusses the key results. Further details

are presented in [16], including the finite element analysis of the test article, descriptions of the test rigs, two critical current predictions for the coil, and additional results.

A. Design of the test article

The key considerations in the design of the test article, apart from producing the correct loading environment, were cost and test rig limitations. To limit cost, only one superconducting coil was to be wound and tested for risk reduction. The main test rig limitation was a limit to the total rotor energy during rotation at the highest test speed, which was established for safety reasons.

Preliminary test article designs that matched the full radius of HEMM's rotor and would almost exactly match the loading conditions for the coil all exceeded the test rig's energy limit by a factor of about 2. To reduce the energy of the test article and maintain the same centrifugal loading, the radius of the test article was reduced relative to HEMM's rotor and the rotational speed of the test was increased. The radius reduction was implemented based on the center of gravity and rotational force on the coil. The center of gravity of the rotor coil was reduced by a factor of 3 and the peak rotational speed of the test article was raised by a factor of $\sqrt{3}$ (from 6,800 rpm to 11,800 rpm). These changes reduced the rotor energy by a factor of 3 while maintaining the total centripetal loading on the coil. However, the direction of the centrifugal loading and the resulting mechanical stress in the coil change as discussed in the next section.

An exploded view of the selected test article design is shown in Fig. 5. The test article consists of:

1) A solid 4340 steel rotor disk meant to mimic the rotor back iron in HEMM and provide appropriate stiffness in the coil test section. 4340 had to be used instead of $Fe_{49.15}Co_{48.75}V_2$, because at room temperature $Fe_{49.15}Co_{48.75}V_2$ has a significantly lower strength than it does at the cryogenic operating temperature of HEMM
2) Two titanium (Ti-6Al-4V, solution heat treated) rotor coil fixture cups that match exactly the coil fixture in the actual HEMM design
3) Four titanium dovetail fixture restraints that are half sections of the dovetail fixtures in the actual rotor
4) Two titanium race track end winding retaining hoops to mimic the end winding retaining hoops in the actual rotor design.
5) Two coils. One test coil and one dummy copper coil

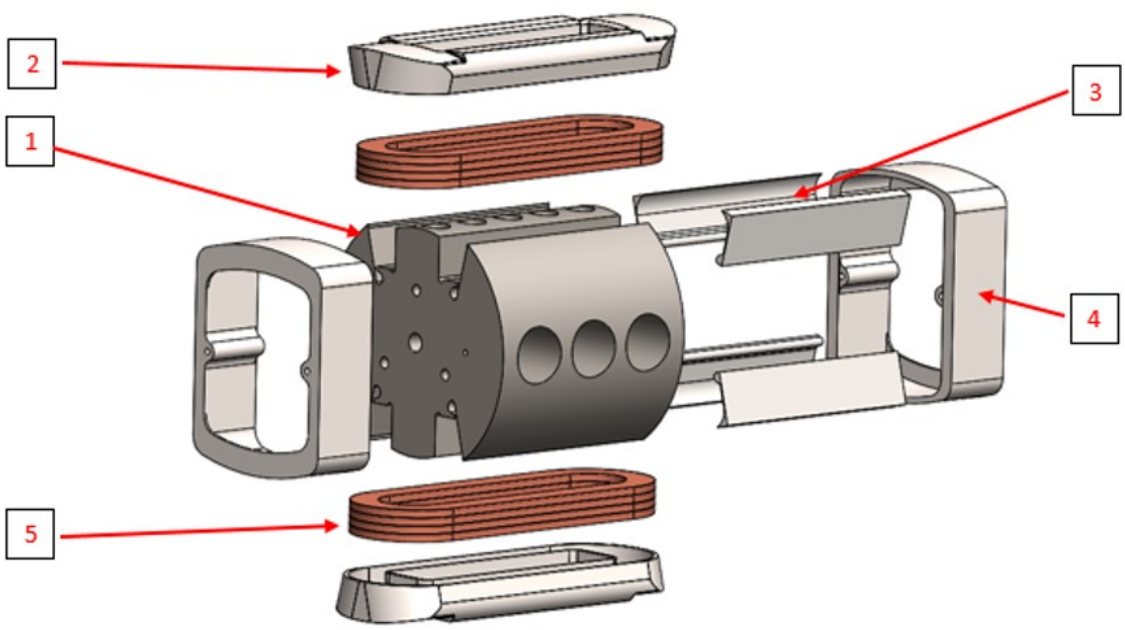

Fig. 5 Exploded View of Key Test Article Components.

The exact geometry of the test article for rotation testing was determined by conducting a (a) 3D structural finite element analysis for the centrifugal loading, (b) comparing the predicted stress tensor components in the superconducting coil to the stress predictions for a model of HEMM with all the thermal, mechanical, and magnetic loads considered, and (c) iterating the geometry until the difference between the two stress predictions was acceptably small. The

superconducting coil was modeled the same way in both cases.

The loading produced by the test article does not exactly match the loading of the full HEMM rotor, because the radius is smaller and because it is tested at room temperature. The smaller radius results in the centripetal load on the coil creating more tangential force and less radial force. The lack of thermal contraction reduces compressive stresses in the coil. The combined result of the above two differences is that in the rotating test the coil experiences some stresses that exceed the peak stresses predicted for the real rotor design.

The coordinate directions of the stress tensor are defined with the 1 direction coincident with the length direction of the superconductor and the 3 direction normal to the face of the superconductor (i.e., coincident with its c-axis). At the maximum test speed of 11,800 rpm, the tensile normal stresses exceed those of the HEMM design by a factor of 1, 1.3, and 4.2, respectively, for the 11, 22, and 33 stress components. At 11,800 rpm, the shear stresses exceed those of the HEMM design by a factor of 1.3, 1.6, and 7.4, respectively, for the 12, 23, and 13 stress components.

Images of the test hardware are shown in Figs. 6 and 7.

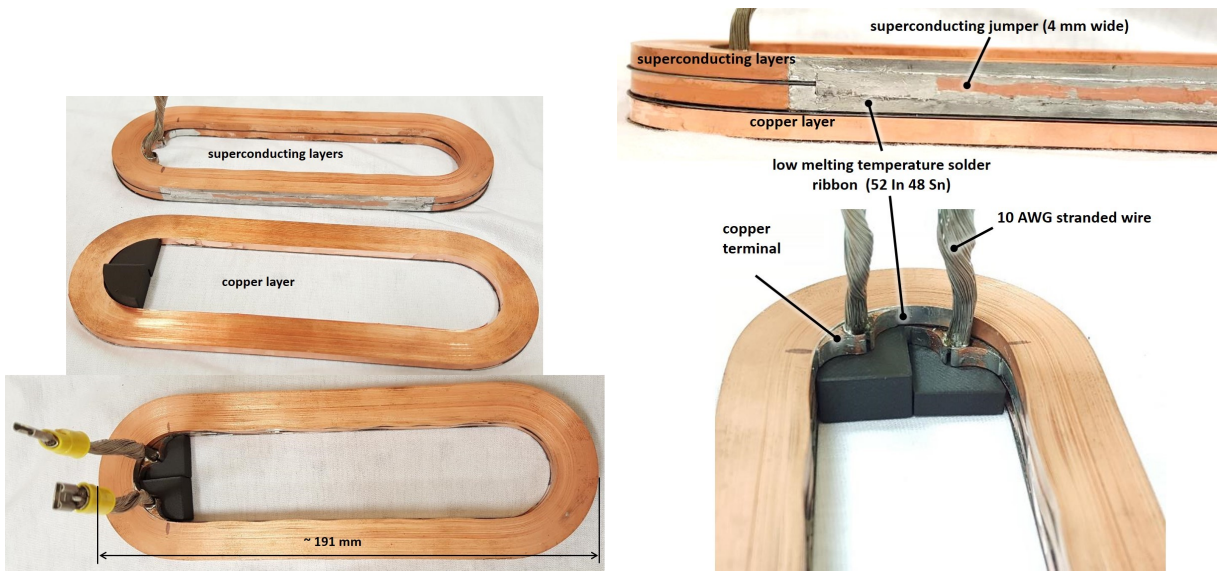

(a) (b)

Fig. 6 Images of the full-scale, two layer superconducting test coil.

B. Test matrix and testing procedure

Stresses in the 23, and 13 direction represent the stresses of most concern in the coil as they are shear stresses that tend to delaminate the layers of the superconductor and the strength of the conductor in these directions is expected to be very low. An exact value for what stress will cause failure in these directions is not known. The test matrix for the rotating test was therefore based off of where the predicted stress in the 23 and 13 directions exceed 5, 10, and 15 MPa. The rationale was that if the coil did fail at a known stress, that stress could be used as the limiting stress in an updated HEMM rotor design. The selected speeds were 4,500, 6,000, 7,500, 9,000, 9,750, and 11,800 rpm. Figure 8 shows all tests speed, balancing speed, and test rig failure speed versus the two critical shear stress predictions.

As before, a summary of the procedure is presented here. The detailed procedure is given in the Appendix. The electrical measurements of the superconductivity response were performed in a manner similar to the procedure used for the thermal cycling test. The differences are as follows. To cool down this test article, it was placed in an empty, room temperature dewar, covered with a lid, and then slowly filled with LN2; this provided a more gradual cool down than the thermal cycling test, because the LN2 boil off cooled the article before it came into direct contact with LN2. After slowly ramping the DC current to each measurement point, a longer dwell was needed (typically about 20 minutes) to ensure that the coil's voltage (an average of 100 readings) was stable. After each electrical measurement, the test article was allowed to warm up to room temperature overnight.

Before rotating the test article, the current leads were taped down to limit movement of the current terminal. The test

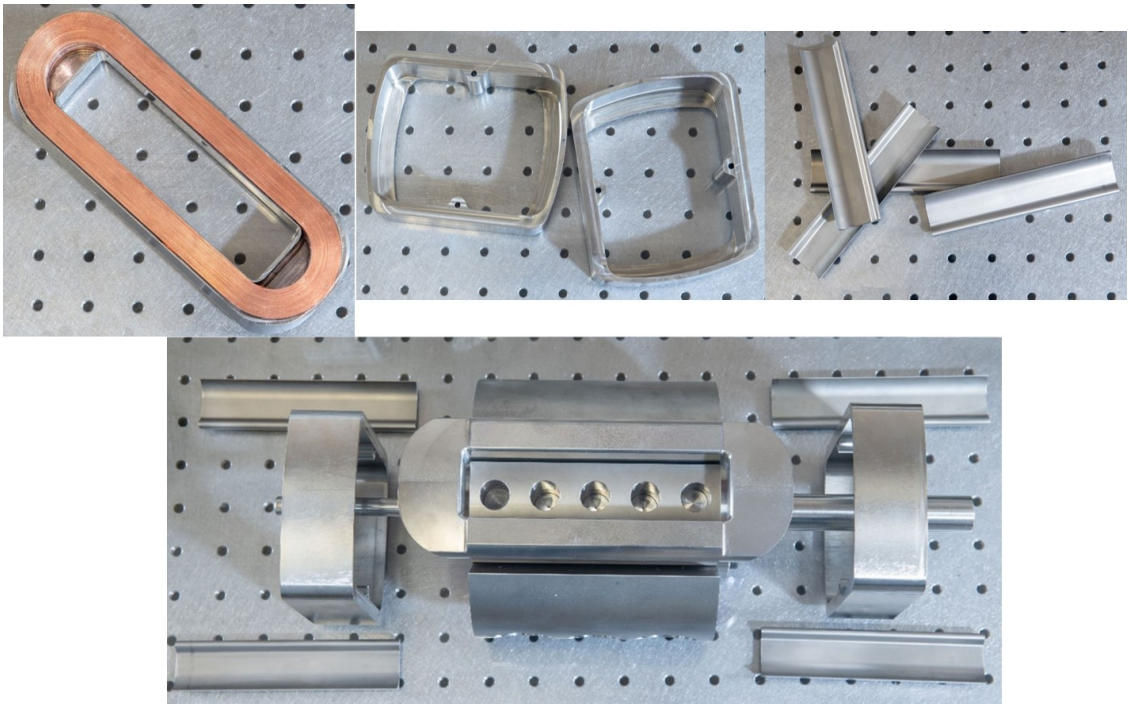

Fig. 7 Images of the fabricated components of the test article.

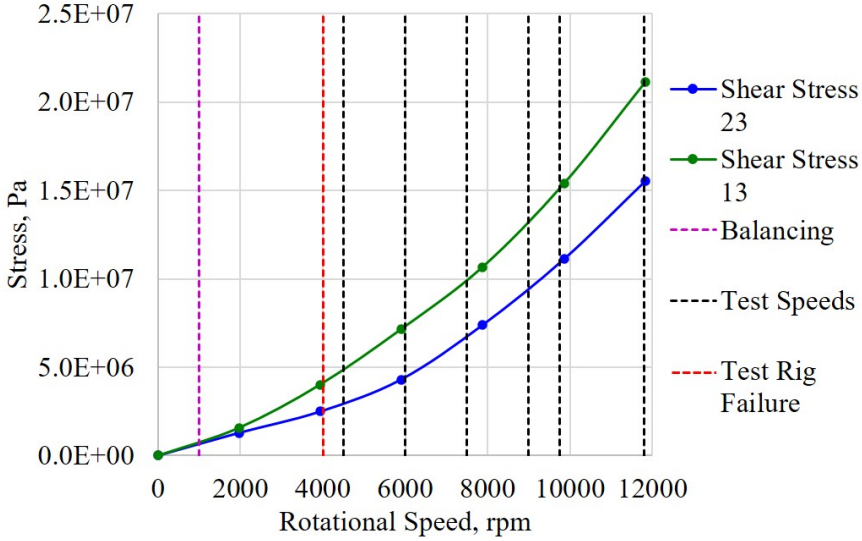

Fig. 8 Critical shear stresses in the coil as a function of the rotational speed of the test article.

article was then mass balanced at 1,000 rpm. Electrical measurements were obtained before and after balancing. Spin testing of the article was initially carried out in a test rig located in-house. However, a coupling failure at 4,000 rpm caused by rotordynamics resulted in failure of that test rig and a large impact load on the test article. All of the subsequent spin tests (6,000 rpm and greater) were carried out at a balancing company.

The coil testing was carried out through progressive spin test at room temperature of the test article to successively higher speed. The coil's superconducting response was measured as described above after each spin test. The aforementioned performance metrics were calculated to assess whether degradation had occurred, as done for the thermal cycling testing.

C. Results and discussion

The measurements that are shown in this section are the measured response of the entire coil (with voltage taps on the current leads) after subtracting the linear Ohmic response caused by the resistive components in the current path (current leads, copper terminals, and solder joints).

To avoid potentially damaging the superconductor due to handling, the test article was not modified in any way or disassembled in any way between the start and end of the rotation tests (from after the initial baseline measurement until after the measurement that followed the 11,800 rpm rotation).

The superconductivity response of the tested coil was measured prior to spin testing and after rotation at each speed. The presence or extent of degradation that was caused by rotation is assessed by visually analyzing the change in the response and quantifying the change in the coil's performance metrics (critical current and n-value). The equivalent operating current for the HEMM coil in this environment (LN2 and self field) is calculated to be 14.1 A, sufficiently below where the voltage becomes appreciable. Therefore, the absolute value of the critical current and n-value metrics is not critical.

A baseline superconductivity measurement was obtained before the test article was rotated. For this baseline measurement, the superconducting coil was installed in the titanium coil fixture, as shown in the top left image in Fig. 7, but not on the steel rotor. After this measurement, the test article was fully assembled and then mass balanced to permit high speed rotation without excessive vibration. The balancing process required that the test article be rotated at 1,000 rpm. Another superconductivity measurement was taken after balancing. These two measurements are shown in Fig. 9.

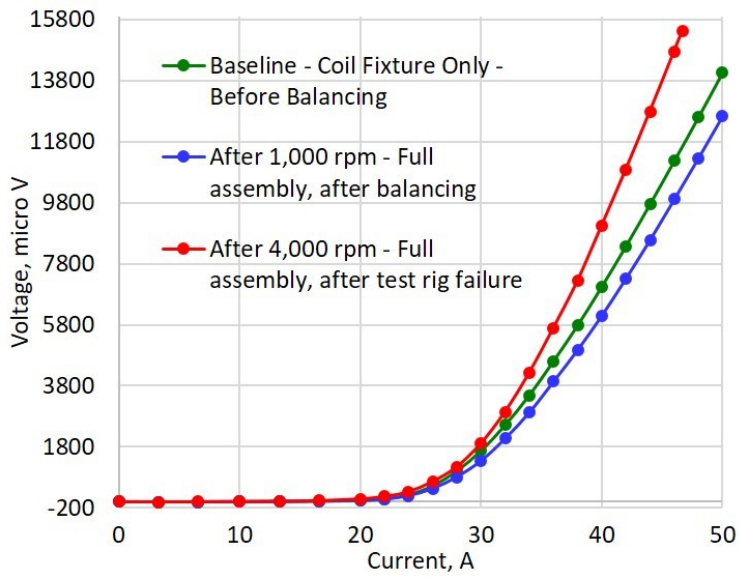

Fig. 9 Baseline measurements of the tested superconducting coil.

The first observation to be made from Fig.9 is that the increase in voltage with current is considerably less steep than expected based on prior testing of similar coils and the predicted response. In particular, the n-value of the baseline response and the response after rotation to 1,000 rpm is about 3.2 and 3.4, respectively. Typically, n-values above 10 or even above 20 are expected. One possible explanation for the low n-value is that the superconductor was damaged during the coil fabrication process. If this were the case, compared to an identical but undamaged coil, the critical current of the damaged coil would be the same or smaller in addition to the n value being smaller. In Fig.9, compared to the predicted response of the coil [16], the n-value is significantly smaller, but the critical current is significantly larger. The coil also exhibits a fully superconducting (i.e., about 0 V) response up to about 20 A, which exceeds one of the predicted critical currents. Thus, damage during coil fabrication does not appear to be a good explanation.

An alternative explanation for the low n-value is that there is a large amount of turn-to-turn current sharing within this no-insulation coil that greatly reduces the total voltage drop across the coil relative to the predicted voltage drop. It is almost certain that current sharing is nonzero, because there was a very tight fit between the superconducting coil and its coil fixture (even before installing the fixture onto the steel rotor). This tight fit should cause a low contact resistance

between turns due to the high contact pressure between turns. The fit was particularly tight on the inner surfaces of the coil at the start of the end turns (i.e., adjacent to the corners of the steel rotor tooth). This is the exact location of the greatest magnitude of the magnetic excitation in the coil. In other words, the turn-to-turn contact resistance is lowest at the location where critical current is expected to be the smallest (and thus where the voltage drop is largest). This would promote turn-to-turn current sharing to distribute the current away from this concentration in the magnetic excitation and reduce the overall voltage drop

The second observation to be made from Fig.9 is that the baseline response and the response after rotation to 1,000 rpm are noticeably different, with the baseline curve having a higher voltage at each current. It is thought that this is due to an increase in turn-to-turn contact pressure (and thus decrease in contact resistance) that resulted from fully assembling the test article. The fit between the coil fixture and both the steel rotor tooth and the dovetail retainers was essentially a press fit. The fixture had to be tapped onto the rotor tooth and then the dovetail retainers had to be carefully hammered into position. Thus, it is reasonable to assume that the contact pressure increased between turns after assembly into the rotor.

After the second superconductivity measurement, an attempt was made to spin the test article to 4,500 rpm in the original test rig. At about 4,000 rpm, a flexible coupling connected to the test article failed, causing the test article to significantly deflect and be thrown off of the shaft on the test article's opposite side. It is important to note that a corner of the test article impacted the test rig's table with enough force to deform the table's surface. Based on the position of certain components and marks on only one corner of the test article, it is believed that the test article impacted the table on a corner of the article that is adjacent to the superconducting coil. Images of the test rig after this failure are shown in Fig. 10. After removing the deformed shaft, the fully assembled test article was tested in liquid nitrogen to determine whether the coil was still operable. Surprisingly, as shown in Fig. 9, the coil still demonstrated a similar, although degraded, superconductivity response. This response still exceeds the required performance of HEMM (after correcting for the magnetic differences between the test article and HEMM) and also provides added confidence in the structural integrity of HEMM's rotor design.

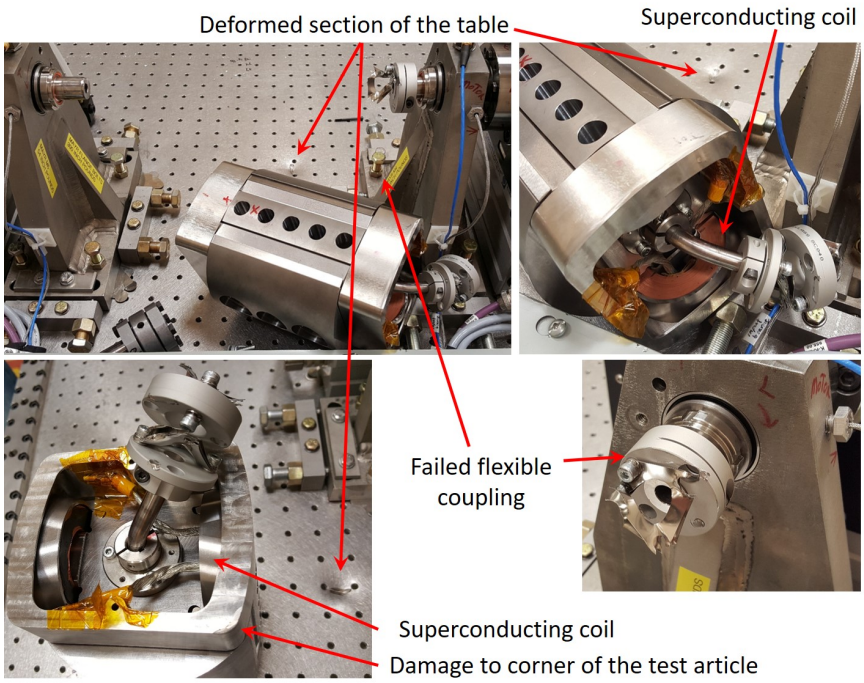

Fig. 10 Images of the test article after failure of the flexible coupling.

Due to the test rig failure and resulting change in superconductivity performance, the baseline response for comparison to subsequent tests had to be re-established as the measured response after the test rig failure. All of the subsequent speed tests are compared to that measurement.

The superconductivity response of the coil was measured after each spin test above 4,000 rpm. These measurements

are depicted in Figs. 11 and 12. From a visual inspection, the responses are very similar to each other in every aspect. There is also no clear trend with speed.

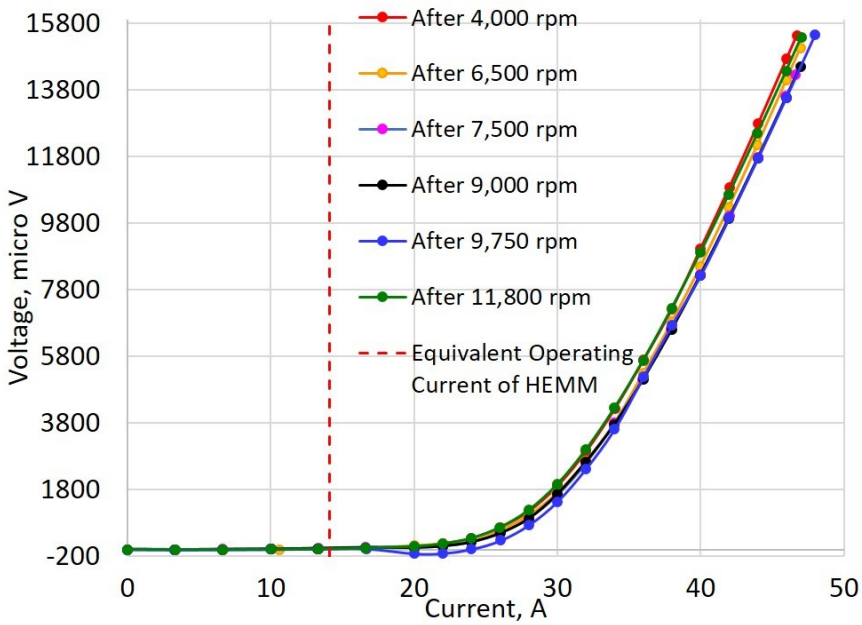

Fig. 11 Voltage versus current responses of the tested coil in the fully assembled test article after room temperature rotations at different speeds.

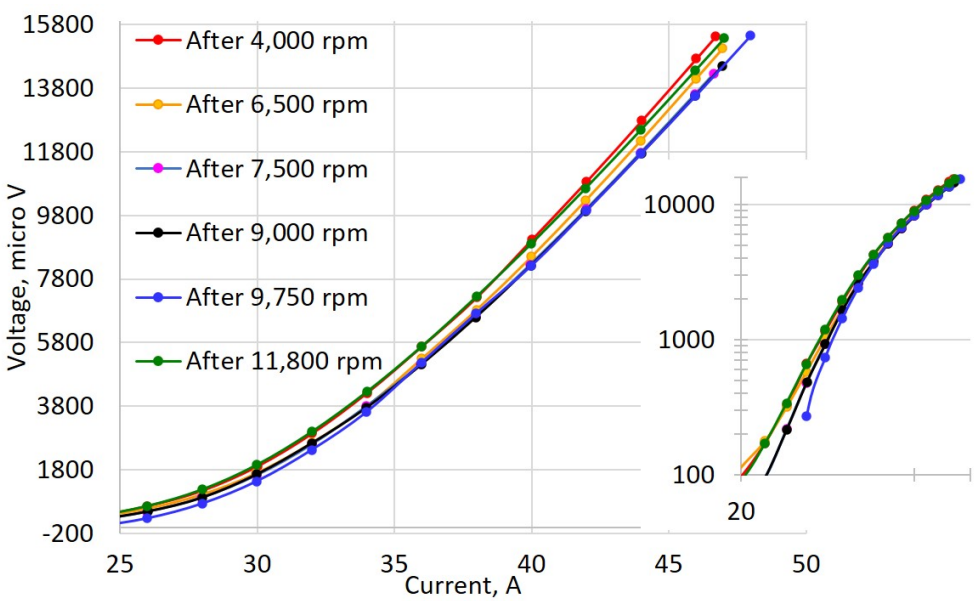

Fig. 12 Voltage versus current responses of the tested coil in the fully assembled test article after room temperature rotations at different speeds.

The critical current and n-value of each curve was calculated. The variation in these performance metrics with rotation speed are shown in Fig. 13. The critical current has an average value of 47.28 A and a span of 1.2 A. The n-value has an average value of 3.64 and a span of 0.40. Although difficult to discern with this few of data points, there does not appear to be a trend in either performance metric. The span of each metric is very small and is very similar to

the span observed in the thermal cycling tests in Section II. It can be concluded from this data that very little, if any, degradation to the coil's superconductivity performance was observed for rotation up to 11,800 rpm.

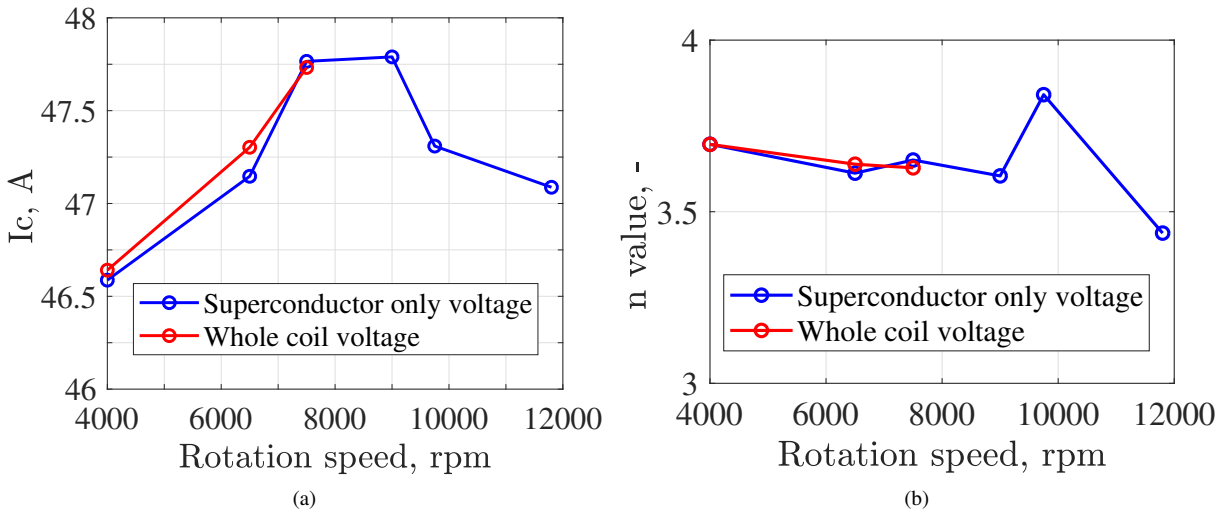

Fig. 13 Change in performance metrics (critical current, left, and n-value, right)) as a function of maximum rotation speed.

Figure 11 also compares the measured responses to the equivalent operating current of HEMM's rotor. This equivalent current was calculated by applying HEMM's rotor design method to the test article used in this experiment. This method uses a critical current interpolation function described in [14]. Here, the interpolation function is generated for the standardized critical current of the superconductor used to wind the coils for this experiment (average value of 103 A according to measurements supplied by the manufacturer). The operating current is determined by first solving a magnetostatic finite element simulation of a design for several values of the current in the superconducting coils. At each value of current, the interpolation function is evaluated to determine the critical current at a given temperature and the magnetic excitation that is produced by that value of current. The operating current is selected to be the value of current at which the current equals the critical current plus a safety factor of 1.5 (i.e., when applied current equals critical current divided by 1.5). For this test article, the equivalent operating current is 14.1 A. This value is significantly lower than HEMM's operating current of about 56 A, because the temperature (77 K) is larger than the operating temperature of HEMM (about 62 K). For this type of superconductor, this difference in temperature results in a significant difference in critical current. In terms of ensuring that HEMM meets its designed performance, a fabricated coil has satisfactory performance if can operate at the equivalent operating current of HEMM without generating excessive heat.

IV. Conclusion

This paper summarized two test campaigns that were undertaken to reduce the risks posed by temperature cycling and high speed rotation on the integrity of the second generation high temperature superconducting coils in NASA's High Efficiency Megawatt Motor (HEMM).

The first campaign was designed to demonstrate that the HEMM coil design could survive repeated thermal cycling from room temperature (293 K) to liquid nitrogen temperature (77 K). The testing method and performance metrics were described. Two coils - a sub-scale, quadruple pancake coil with 25 turns per layer and a full-scale, double pancake coil with 221 turns per layer – were fabricated and tested. The sub-scale coil experienced temporary degradation due to partial detachment of a current terminal. After reattaching the current lead, the performance metrics returned to their pre-damage levels for another 37 cycles, indicating that the degradation was restricted to the physical connection between the current terminal and superconductor rather than degradation of the superconductor itself. The relevant solder joint was improved in subsequent coils and a purpose-built fixture was designed to improve the solder joint in future coils. Apart from the aforementioned temporary degradation, there are no clear trends in the calculated performance metrics. The observed variation in the metrics is small (less than 1.5 A in the critical current and less than 3.5 in the n-value), particularly when considering the experimental uncertainty. A line was fit to the data from the coil

that was thermally cycled 50 times. The slope of the linear fit is negative for both the critical current and n value but each has a third-digit magnitude that may not be statistically significant if the experimental uncertainty is considered (particularly for the n-value). Further, the measured critical currents of these coils fall within the range predicted by finite element simulations of these coils [14]. Consequently, the results indicate that full-scale superconducting coils manufactured in-house for the rotor of HEMM can reliably survive repeated thermal cycling with no or acceptably slow degradation.

The purpose of second risk reduction experiment was to either (a) demonstrate that a no-insulation superconducting coil could maintain performance under the mechanical loading environment of the HEMM rotor design or (b) quantify the limiting speed and stresses that the coil could sustain without appreciable degradation. This testing was performed by spin testing a full-scale HEMM coil on a representative rotor structure at room temperature and sequentially higher rotation speeds and measuring the superconductivity response of the coil at liquid nitrogen temperatures before and after each spin test. Tests were carried out to the full centrifugal loading of a recent HEMM design. According to finite element analysis, this load produced stress components in the coil that exceed their design limit by a factor of 1 to 7.4. Although not yet confirmed, the current HEMM design is expected to produce even smaller stresses in the coil due to a 20% reduction in the coil's mass and an increased volume of structural material. The only degradation of the coil that occurred during this testing resulted from a test rig failure and the voltage taps that are not part of the final coil design.

It was also noted in testing that the coil's superconductivity response had a much lower n-value than would be expected for a short, straight segment of the same conductor or a fully insulated and undamaged coil produced from the same conductor. It is believed that current sharing between turns of a no-insulation coil results in this lower observed n-value for the coil. Further investigation and model development is needed to verify that this is the case. The equivalent operating point of the HEMM coils in this test is sufficiently below the knee in the superconductor's electrical response. Below the knee, changes in n-value have an insignificant effect on the coil's total voltage and energy dissipation. Consequently, a robust explanation of this lower n-value is deemed not required to validate that HEMM's rotor design will survive the loads that it is expected to be subjected to.

Appendix

Procedure for thermal cycling tests

The testing procedure was as follows:

1) Turn on the amplifier and multimeter and let them warm up for at least 15 minutes.
2) Fill the dewar with LN2 to a level that will fully submerge the coil throughout the test.
3) Very slowly lower the coil into the LN2 pool. This process should take about 1.5 to 2 minutes.
4) Connect the amplifier to the coil's current terminals. Connect a 6 1/2 digit multimeter to the voltage tap leads.
5) Set the voltage limit on the linear amplifier to 1.5 V.
6) Set the amplifier to current control mode.
7) Slowly increase the DC current in steps until the measured voltage just exceeds the voltage at the critical current (as defined by the standard electric field criterion).
    1) For the full-size coil, the ramps between DC current levels need to be even slower (about 0.1 A/s) to minimize heating in the coil due to AC losses and turn-to-turn current flow.
8) At each DC current level, wait for the voltage reading the reach steady state, then record the voltage.
    1) Particularly at currents near the critical current, the voltage in steady state may vary within a reasonably small range; in these cases, the average reading in steady state should be used.
9) Slowly decrease the DC current in steps until the current reaches zero. Use the same current ramp rates as in step 7.
10) Post process the data to calculate the performance metrics.
11) Thermally cycle the coil
    1) Remove the coil from the pool of LN2 and let it air quench for about 5 minutes.
    2) Hold the coil in front of a relatively large and high-speed fan for about 4 or 5 minutes (approximately 1 to 2 minutes after the condensation has evaporated off the coil).
    3) Very slowly lower the coil into the LN2 pool. This process should take about 1.5 to 2 minutes.
    4) Wait about 5 minutes for the coil to reach a steady state temperature
12) If a measurement will not be taken at this thermal cycle, repeat step 11. Otherwise repeat steps 7 through 11.

Procedure for high speed rotation tests

The testing procedure was as follows:

1) Test article is prepped for spin test by taping down coil wire leads
2) Test article is delivered to spin test rig either in-house or via shipment to the balancing company.
3) Test article is assembled into spin rig
4) Test article is accelerated to test speed
5) Test speed is maintained for > 10 s but no longer than 1 min
6) Test article is decelerated
7) Test article is delivered to an in-house coil cryogenic testing rig.
8) Test article is prepared for coil testing by adding wire leads and assembling testing fixture
9) Test article is place in empty liquid nitrogen dewar
10) The dewar is filled with liquid nitrogen
11) Current is applied to the coil in progressive interval and voltage measurements are taken
    1) Current is ramped slowly between test points (<.1 A/s)
    2) The coil is allowed to settle at the applied current before a voltage measurement is taken. (typically on the order of 20 min)
    3) Coil testing is stopped when the coil reaches its critical current or the limits of the power supply
    4) Current is ramped down on the coil slowly.
12) The Test Article is removed from the liquid nitrogen and allowed to warm up overnight
13) Steps 1 through 12 are repeated for all test speeds.

Acknowledgments

This work is sponsored by the NASA Advanced Air Transportation Technologies Project - Propulsion & Power Subproject managed by Amy Jankovsky, and the Convergent Aeronautics Solutions Project - High Efficiency Electrified Aircraft Thermal Research (HEATheR) activity.

References

[1] Tallerico, T. T., Scheidler, J. J., Lee, D., and Haran, K., "Electromagnetic redesign of NASAs high efficiency megawatt motor," *2020 AIAA/IEEE Electric Aircraft Technologies Symposium (EATS)*, IEEE, 2020, pp. 1–15. doi:10.2514/6.2020-3600.

[2] Jansen, R. H., Scheidler, J., Tallerico, T., Kascak, P., Woodworth, A., Smith, A. D., Dyson, R., Sixel, W., Thompson, J., Stalcup, E., et al., "High efficiency megawatt motor risk reduction activities," *2020 AIAA/IEEE Electric Aircraft Technologies Symposium (EATS)*, IEEE, 2020, pp. 1–12.

[3] Jansen, R. H., Kascak, P., Dyson, R., Woodworth, A., Scheidler, J., Smith, A. D., Stalcup, E., Tallerico, T., De Jesus-Arce, Y., Avanesian, D., et al., "High Efficiency Megawatt Motor Preliminary Design," *2019 AIAA/IEEE Electric Aircraft Technologies Symposium (EATS)*, IEEE, 2019, pp. 1–13. doi:10.2514/6.2019-4513.

[4] Scheidler, J. J., Tallerico, T. F., Miller, W. A., and Torres, W., "Progress Toward the Critical Design of the Superconducting Rotor for NASA's 1.4 MW High-Efficiency Electric Machine," *2019 AIAA/IEEE Electric Aircraft Technologies Symposium (EATS)*, IEEE, 2019, pp. 1–13. doi:10.2514/6.2019-4496, URL `https://ntrs.nasa.gov/citations/20190032029`.

[5] Scheidler, J. J., and Tallerico, T. F., "Design, Fabrication, and Critical Current Testing of No-Insulation Superconducting Rotor Coils for NASA's 1.4 MW High-Efficiency Megawatt Motor," *2018 AIAA/IEEE Electric Aircraft Technologies Symposium (EATS)*, IEEE, 2018, pp. 1–9.

[6] Jansen, R., De Jesus-Arce, Y., Kascak, P., Dyson, R. W., Woodworth, A., Scheidler, J. J., Edwards, R., Stalcup, E. J., Wilhite, J., Duffy, K. P., et al., "High efficiency megawatt motor conceptual design," *2018 Joint Propulsion Conference*, 2018, p. 4699. doi:10.2514/6.2018-4699.

[7] Scheidler, J. J., "Preliminary Design of the Superconducting Rotor for NASA's 1.4 MW High-Efficiency Electric Machine," *2018 Joint Propulsion Conference*, 2018, p. 4617.

[8] Oomen, M., Herkert, W., Bayer, D., Kummeth, P., Nick, W., and Arndt, T., "Manufacturing and test of 2G-HTS coils for rotating machines: Challenges, conductor requirements, realization," *Physica C: Superconductivity and its applications*, Vol. 482, 2012, pp. 111–118. doi:10.1016/j.physc.2012.04.021.

[9] Zhang, Y., Hazelton, D., Knoll, A., Duval, J., Brownsey, P., Repnoy, S., Soloveichik, S., Sundaram, A., McClure, R., Majkic, G., et al., "Adhesion strength study of IBAD–MOCVD-based 2G HTS wire using a peel test," *Physica C: Superconductivity*, Vol. 473, 2012, pp. 41–47. doi:10.1016/j.physc.2011.11.013.

[10] Barth, C., Bagrets, N., Weiss, K., Bayer, C., and Bast, T., "Degradation free epoxy impregnation of REBCO coils and cables," *Superconductor Science and Technology*, Vol. 26, No. 5, 2013, p. 055007. doi:10.1088/0953-2048/26/5/055007.

[11] Duan, Y., and Gao, Y., "Delamination and current-carrying degradation behavior of epoxy-impregnated superconducting coil winding with 2G HTS tape caused by thermal stress," *AIP Advances*, Vol. 10, No. 2, 2020, p. 025320. doi:10.1063/1.5134925.

[12] Park, H. J., Kim, Y.-c., Moon, H., Park, M., and Yu, I., "Improvement of Degradation Characteristics in a Large, Racetrack-shaped 2G HTS Coil for MW-class Rotating Machines," *Journal of Electrical Engineering and Technology*, Vol. 13, No. 3, 2018, pp. 1166–1172. doi:10.5370/JEET.2018.13.3.1166.

[13] Hazelton, D. W., "SuperPower 2G HTS conductor," *1st Workshop on Accelerator Magnets in HTS*, 2014.

[14] Scheidler, J. J., Tallerico, T. F., Miller, W. A., Torres, W., and Mulder, T. T., "Thermal cycling testing of stationary superconducting rotor coils for the High Efficiency Megawatt Motor (HEMM)," NASA Technical Memo, 2022 (in preparation).

[15] Ekin, J., *Experimental techniques for low-temperature measurements: cryostat design, material properties and superconductor critical-current testing*, Oxford university press, 2006.

[16] Scheidler, J. J., and Tallerico, T. F., "Superconducting Coils Under High Speed Rotation," NASA Technical Memo, 2022 (in preparation).